HAL
open science

The summit hydrothermal system of Stromboli: New insights from self-potential, temperature, CO2 and fumarolic fluids measurements, with structural and monitoring implications.

Anthony Finizola, Francesco Sortino, Jean-François Lénat, Maurice Aubert, Maurizio Ripepe, Mariano Valenza

To cite this version:

Anthony Finizola, Francesco Sortino, Jean-François Lénat, Maurice Aubert, Maurizio Ripepe, et al.. The summit hydrothermal system of Stromboli: New insights from self-potential, temperature, CO2 and fumarolic fluids measurements, with structural and monitoring implications.. Bulletin of Volcanology, 2003, 65, pp.486-504. 10.1007/s00445-003-0276-z . hal-01452541

HAL Id: hal-01452541

https://hal.science/hal-01452541

Submitted on 2 Feb 2017

HAL is a multi-disciplinary open access archive for the deposit and dissemination of scientific research documents, whether they are published or not. The documents may come from teaching and research institutions in France or abroad, or from public or private research centers.

L'archive ouverte pluridisciplinaire **HAL**, est destinée au dépôt et à la diffusion de documents scientifiques de niveau recherche, publiés ou non, émanant des établissements d'enseignement et de recherche français ou étrangers, des laboratoires publics ou privés.

The summit hydrothermal system of Stromboli. New insights from self-potential, temperature, CO_2 and fumarolic fluid measurements, with structural and monitoring implications

Anthony Finizola · Francesco Sortino · Jean-François Lenat · Maurice Aubert· Maurizio Ripepe · Mariano Valenza

Abstract Accurate and precisely located self-potential (SP), temperature (T) and CO_2 measurements were carried out in the summit area of Stromboli along 72 straight profiles. SP data were acquired every metre and T data every 2.5 m. CO_2 concentrations were acquired with the same density as T, but only along seven profiles. The high density of data and the diversity of the measured parameters allows us to study structures and phenomena at a scale rarely investigated. The shallow summit hydrothermal activity (Pizzo–Fossa area) is indicated by large positive SP, T and CO_2 anomalies. These anomalies are focused on crater faults, suggesting that the fracture zones are more permeable than surrounding rocks at Stromboli. The analysis of the distribution of these linear anomalies, coupled with the examination of the geologic, photographic and topographic data, has led us to propose a new structural interpretation of the summit of Stromboli. This newly defined structural framework comprises (1) a large Pizzo circular crater, about 350 m in diameter; (2) a complex of two concealed craters nested within the Pizzo crater (the Large and the Small Fossa craters), thought to have formed during the eruption of the Pizzo pyroclastites unit; the Small Fossa crater is filled with highly impermeable material that totally impedes the upward flow of hydrothermal fluids; and (3) The present complex of active craters. On the floor of the Fossa, short wavelength SP lows are organized in drainage-like networks diverging from the main thermal anomalies and converging toward the topographic low in the Fossa area, inside the Small Fossa crater. They are interpreted as the subsurface downhill flow of water condensed above the thermal anomalies. We suspect that water accumulates below the Small Fossa crater as a perched water body, representing a high threat of strong phreatic and phreatomagmatic paroxysms. T and CO_2 anomalies are highly correlated. The two types of anomalies have very similar shapes, but the sensitivity of CO_2 measurements seems higher for lowest hydrothermal flux. Above T anomalies, a pronounced high frequency SP signal is observed. Isotopic analyses of the fluids show similar compositions between the gases rising through the faults of the Pizzo and Large Fossa craters. This suggests a common origin for gases emerging along different structural paths within the summit of Stromboli. A site was found along the Large Fossa crater fault where high gas flux and low air contamination made gas monitoring possible near the active vents using the alkaline bottle sampling technique.

A. Finizola (✉) · J.-F. Lénat · M. Aubert
Laboratoire Magmas et Volcans, OPGC,
Université Blaise Pascal, CNRS,
5 rue Kessler, 63038 Clermont-Ferrand, France
e-mail: finizola@ov.ingv.it
Tel.: +39-81-6108357
Fax: +39-81-6108351

F. Sortino · M. Valenza
Istituto Nazionale di Geofisica e Vulcanologia (INGV),
Via Ugo La Malfa, 153, 90144 Palermo, Italy

M. Ripepe
Dipartimento di Scienze della Terra,
Università di Firenze, Via Giorgio La Pira 4, 50121 Firenze, Italy

M. Ripepe
Laboratorio di Geofisica, Dipartimento di Scienze della Terra,
Università degli Studi di Camerino,
Via Gentile III da Varano, 62032 Camerino (MC), Italy

M. Valenza
Dipartimento di Chimica e Fisica della Terra e Applicazioni,
Università di Palermo, Via Archirafi, 36, 90123 Palermo, Italy

Present address:
A. Finizola, Osservatorio Vesuviano,
INGV sezione di Napoli, via Diocleziano 328, 80124 Napoli, Italy

Introduction

Active hydrothermal systems usually develop on active volcanoes in response to the circulation of magmatic gases, heat and meteoric water. They dissipate much of the volcanic energy and are often the sites of the first indications of impending crises. Their study is also important in investigations of the circulation of heat and fluids inside the edifices and in the development of monitoring techniques. Stromboli volcano is an ideal place for such studies. Its activity is long-lived and the presence of a very active hydrothermal system at its summit is evident from surface hydrothermal alteration, warm ground and fumaroles. As far as volcanic risk is concerned, a better understanding of the eruptive mechanisms of this volcano is important because paroxysmal explosions occur periodically, threatening large parts of the island (Barberi et al. 1993). Since 1989, the Osservatorio di Firenze has studied the explosive mechanisms of Stromboli using seismic, acoustic, infrasonic, thermal monitoring and video camera data (e.g. Ripepe et al. 1993, 1996, 2001; Braun et al. 1996; Ripepe 1996; Ripepe and Gordeev 1999). In addition, a network of the Istituto Nazionale di Geofisica e Vulcanologia of Catania involves video camera, seismic, tilt measurements and GPS monitoring (Alparone et al. 1999; Bertagnini et al. 1999; Bonaccorso et al. 1999; Coltelli et al. 1999). However, it has not yet been possible to detect clear precursors before the 17 major explosive events that have occurred since the beginning of the monitoring. The monitoring of other parameters, such as the composition of volcanic gases or the geothermal flux could help in understanding the onset of the rapid variations in the intensity of the explosions.

Some limited geophysical and geochemical surveys have been carried out at the summit of Stromboli. Ballestracci (1982a, 1982b) suggests the presence of several convective cells associated with SP positive anomalies close to the active craters in the Fossa area. Carapezza and Federico (2000) have reported the results of yearly measurements, since 1992, of dry gas sampling in the Pizzo area.

Our study focuses on the hydrothermal system around the active craters. We use simultaneous self-potential (SP), temperature (T) and soil gas measurements because of their relevance to hydrothermal activity. In volcanic areas, hydrothermal systems usually generate high amplitude positive SP anomalies (Zablocki 1976; Aubert et al. 1984; Aubert and Dana 1994; Di Maio and Patella 1994; Malengreau et al. 1994; Zlotnicki et al. 1994; Patella 1997; Finizola et al. 1998; Lénat et al. 1998). They are mainly generated by streaming potential (Corwin and Hoover 1979) related to shallow water flow in the hydrothermal system. CO_2 anomalies have their origin in the exsolution from magma at depths of several kilometres (Papale 1999). Structural surveys using CO_2 or He, in flux or concentration, in soil gases have succeeded in finding anomalies in zones often corresponding to faults (Aubert and Baubron 1988; D'Alessandro et al. 1992; Barberi and Carapezza 1994; Giammanco et al. 1997, 1998; Allard et al. 1998; Azzaro et al. 1998; Etiope et al. 1999). T anomalies rely on conductive and convective heat transfers. Our survey is composed of detailed SP, T and CO_2 soil gas concentration measurements and of several fluid geochemistry stations.

Geological setting

Stromboli is located in the Tyrrhenian Sea, in the northernmost part of the Aeolian archipelago. Submarine investigations in the Stromboli area (Gabbianelli et al. 1993) identified a predominant regional NE–SW structural trend, also displayed in the subaerial part of the edifice by preferential dyke orientation (Zanchi and Francalanci 1989; Pasquarè et al. 1993; Fig. 1). Geological surveys (Rosi 1980; Francalanci 1987; Zanchi and Francalanci 1989; Keller et al. 1993) show that the subaerial evolution of Stromboli Island began 100 ka ago and can be divided into seven phases, separated by erosional deposits or by collapses of calderas or flanks (Hornig-Kjarsgaard et al. 1993; Pasquarè et al. 1993). These phases occurred during the two main stages of the evolution of Stromboli (Pasquarè et al. 1993). The first one, from 100 to 21 ka, comprises a series of pyroclastic eruptions associated with a flank collapse toward the SE and with three caldera collapses (PalaeoStromboli I, II, III, Scari and lower Vancori cycle). During the second stage, from 21 ka to the present (middle and upper Vancori, NeoStromboli and Recent Stromboli cycle), the activity has been predominantly effusive.

The transition between the NeoStromboli and the Recent Stromboli cycle occurred most probably ca. 5,000 years B.P. (Gillot 1984; Gillot and Keller 1993). Two major events are associated with this transition ; (1) a sector collapse which formed the Sciara del Fuoco depression (no° 1 in Fig. 1) and probably also the Rina Grande sector collapse (no° 2 in Fig. 1), and (2) the collapse of the Fossetta crater (no° 3 in Fig. 1) of which only the south-western part remains preserved as the present-day Fossetta depression (Hornig-Kjarsgaard et al. 1993).

Activity on the Recent Stromboli cycle is divided into three periods (Hornig-Kjarsgaard et al. 1993).

1. The Pizzo Sopra la Fossa (or Pizzo) pyroclastites event (no° 4 in Fig. 1, and no° 3 in Fig. 2), related to the formation of a nested tuff cone within the larger Fossetta crater, at the head of the Sciara collapse.
2. An effusive period filling the Fossetta crater with lava flows before the Sciara collapse had reached its present extent. The lava flow sequence crops out in the steep cliffs facing the Sciara del Fuoco, SW of the present active craters.

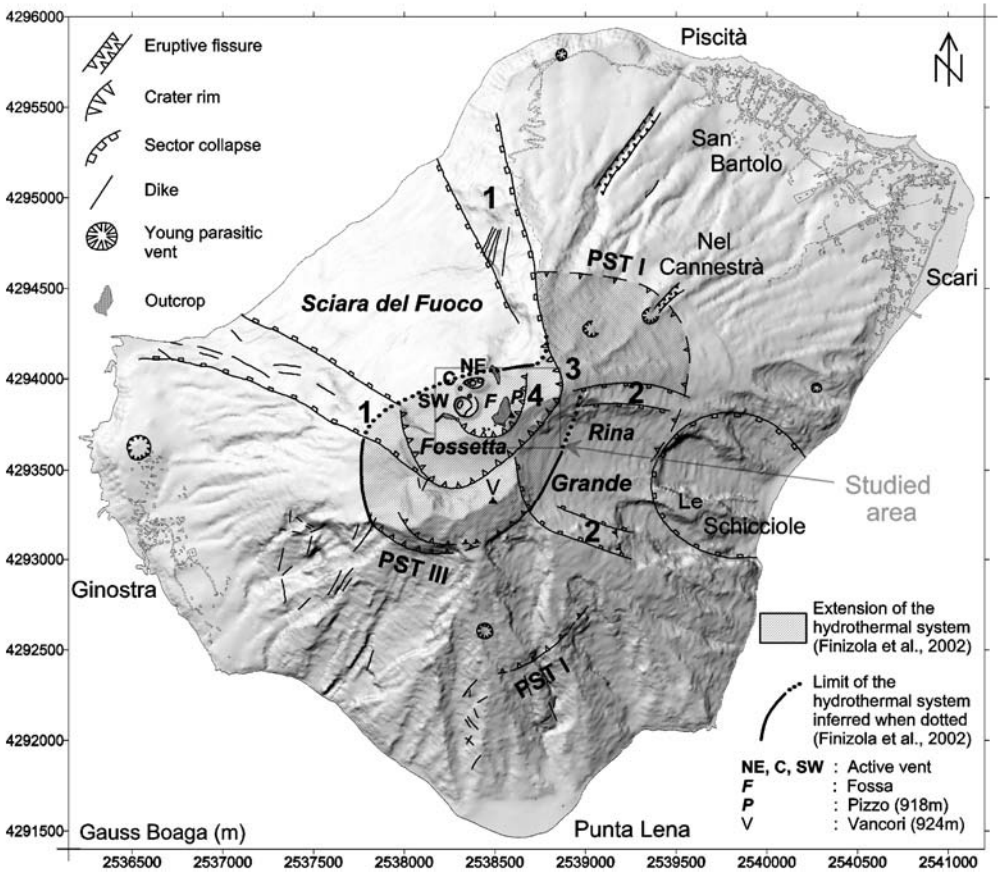

Fig. 1 Shaded relief map of Stromboli island (illumination from the NW) showing the study area at the summit, the extent of the general hydrothermal system (after Finizola et al. 2002) and the main volcano-structural features (after Pasquarè et al. 1993; Keller et al. 1993). *Numbers* designate structures discussed in the text

3. The Sciara lavas and summit tephra from present activity.

Our survey zone (Fig. 2) is located in the upper part of the Sciara del Fuoco collapse and can be divided into three sections.

1. The Pizzo area, which culminates at 918 m above sea level (a.s.l.).
2. The Fossa, a platform at approximately 800 m a.s.l.
3. The active craters.

Two main types of rock are present at the surface (Figs. 2 and 3): (1) an accumulation of tephra from the recent and present-day strombolian activity at the active craters, and (2) outcrops of pyroclastites and/or massive lava, recognized in seven places in the study area (no° 1 to 7 in Fig. 2). In the Fossa area, outcrops 3 to 6 (Figs. 2 and 3), are well-stratified pyroclastites with several units separated by unconformities, and a general dip toward the present active craters. They are strongly altered by fumarolic activity (Hornig-Kjarsgaard et al. 1993). These formations (outcrops 3, 4, 5 and 6), named Pizzo Sopra la Fossa Pyroclastites in the literature, will be referred to as the Pizzo pyroclastites herein. In the Sciara del Fuoco area, three other outcrops (1, 2 and 7 in Fig. 2) display more heterogeneous characteristics. Outcrop 1 consists of pyroclastic deposits intersected by lava (lava flows or sills). Outcrop 2 is not well defined due to strong alteration by NE crater fumarolic activity, but it seems to essentially consist of pyroclastic deposits. Outcrop 7 can be divided into four parts: (1) the upper 10 m are white, intensely altered rocks showing essentially fumarolic minerals (pickeringite and gypsum). (2) Most of the outcrop, ESE–WNW in direction, consists of pyroclastic layers in the southern part and (3) lava flows in the northern part. (4) The lower part of the outcrop, NE–SW in direction, displays pyroclastic deposits cut by a thick dike.

The active craters comprise two main craters, (NE and SW in Fig. 2), separated by two mildly active vents constituting the central crater (C in Fig. 2). Present-day strombolian activity is mostly concentrated in the NE and SW craters.

Sources of T, SP and CO_2 anomalies

Surface thermal anomalies are generally linked to shallow hydrothermal systems in the upper parts of active volcanoes. In the absence of fumarolic activity at the surface, the rise of hot fluids in convective cells can be detected by soil temperature elevation because the condensation of water steam at depth releases large quantities of heat. Thermal anomalies, thus, are thought to

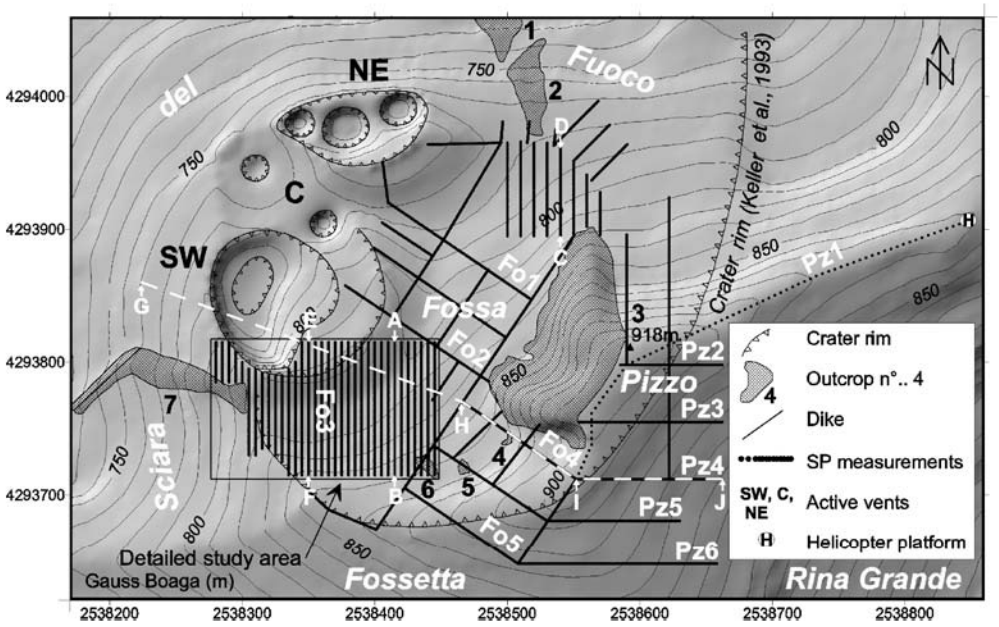

Fig. 2 Shaded relief map of the study area. Contours and spot heights are in metres. *Numbers 1–7* are outcrops (*hatched pattern*) discussed in the text. *Black dots or lines* represent the different measurement profiles. *Fo1, Fo2, etc.* and *Pz1, Pz2, etc.* designate the Fossa and Pizzo profiles, respectively. *Letters* (*A, B, C, D...*) correspond to the location of the (*A–B, C–D...*) profiles shown in Figs. 7 and 8

coincide with permeable zones where uprising hot fluids escape preferentially.

The interpretation of the SP anomalies is less straightforward because several mechanisms can produce SP signals. On volcanoes, two main mechanisms are generally considered: electrokinetic and thermoelectric coupling (Corwin and Hoover 1979), but theoretical considerations and observation suggest that electrokinetic potential is significantly larger than thermoelectric potential. Electrokinetic potentials are created by fluid flow in porous media (here the volcanic edifice). In the absence of a hydrothermal system, fluid flow will be restricted to the mostly vertical flow of vadose water towards a water table. The linear reverse relationship between SP and altitude commonly observed on the flanks of volcanoes is thought to be related to an increase in thickness of the vadose zone with altitude (Zablocki 1978; Schiavone and Quarto 1984; Ernstson and Scherer 1986; Jackson and Kauahikaua 1987; Aubert and Atangana 1996; Aubert et al. 1990, 1991, 1993). At Kilauea volcano, Jackson and Kauahikaua (1987) showed that this relationship can be used to detect water table depth. In this case, SP lows correspond to maximum thicknesses of the unsaturated zone. In the presence of a hydrothermal system, uprising fluids will generate positive SP anomalies (Zablocki 1976; Nishida and Tomiya 1987; Aubert and Baubron 1988; Matsushima et al. 1990; Aubert 1999). Therefore, an ambiguity will exist in the interpretation of SP highs. If the system is purely hydrogeological, a SP high can be interpreted as the rise of the water table (for example in the presence of impermeable layers). But if a hydrothermal system is present, a SP high can also correspond to the upward flow of fluids in a convective cell. The ambiguity can sometimes be resolved if the SP reference is taken on a basal water table (an aquifer or the sea). The value of this reference potential is the upper limit for the potentials generated by hydrogeological processes. Positive values, therefore, will indicate the contribution of a hydrothermal component. Coupling SP measurements with other types of data, such as temperature and CO_2, will generally help to resolve the ambiguities in the interpretation of SP anomalies.

On active volcanoes, CO_2 anomalies are generally associated with highly permeable zones, which may also drain heat and other fluids. Indeed, surveys coupling soil gas and T measurements over active fissures show a good correlation between these parameters (e.g. Aubert and Baubron 1988).

Data acquisition and processing

SP, T and CO_2 data

SP, T measurements and soil gas sampling were carried out at the summit (Fig. 1) during two preliminary field campaigns in May 1992 and August 1994, and field campaigns in July–August 1995, April 1996 (Finizola 1996) and August 1999. 6086 SP, 2746 T and 377 soil gas measurements were made along 72 straight profiles (Fig. 2). In order to measure the different parameters (SP, T, soil gas) at exactly the same locations, and to achieve dense and regular sampling, a network of benchmarks (wooden markers) spaced 5 m apart in plan view were installed (Fig. 3). The benchmark network was also used to map the Pizzo pyroclastite outcrops and crater rims accurately.

SP data were acquired every 1 m and T measurements every 2.5 m along the 72 profiles. Soil gas concentration measurements were acquired at the same sites as T measurements, but only along seven profiles (Fo1 to Fo5, Pz2 and Pz4 profiles in Fig. 2). In the southern part of the

Fig. 3 Photograph showing the topographic techniques used during the field campaign with benchmarks (wooden markers) spaced 5 m apart in plan view. *Red and blue markers* correspond, respectively, to topographic reference and thermal sensors. *F1* and *F3* represent the maxima of T anomalies. The area displayed two kinds of lithology, the strombolian tephra in the foreground and the pyroclastite outcrops (*pink numbers 3–6*). Anomaly and outcrop descriptions are as in previous figures

SW crater (Fig. 2), an area 165×100 m was the object of a very detailed study, including 34 parallel N–S profiles spaced 5 m apart.

The SP equipment consisted of a high-impedance voltmeter, a pair of $Cu/CuSO_4$ non-polarizing electrodes and an insulated electric cable. The potential of the sea was taken as the reference potential using a station (Gauss Boaga 4293687 N, 2538370°E) common to this survey and a SP survey covering the entire Stromboli Island (Finizola et al. 2002). The electrical contact with the ground was always good (always <200 kΩ and generally <20 kΩ) because moisture was found a few centimetres below the surface. Closures of the profiles were made as frequently as possible, and closure errors were always lower than 10 mV.

Thermal probes and a digital thermometer were used for the ground temperature measurements. Readings were taken to a tenth of a degree. Each T measurement was done in four steps: (1) burrowing of a hole at a precise depth of 30 cm with a steel rod, 2 cm in diameter; (2) insertion of a thermal probe into the hole at the precise depth of 30±1 cm by means of a graduated wooden stick; (3) filling and compaction of the hole; and (4) a temperature reading was taken after 10–15 min (in order to achieve thermal equilibrium). A 1.1 °C diurnal temperature variation was measured during one summer day at 30 cm depth in an area outside the thermal anomalies. This provides a crude estimate of the diurnal wave amplitude at the considered depth.

CO_2 emanation data can be obtained by two different types of measurements: concentration or flux. Etiope et al. (1999) find that a general linear relationship exists between concentration and flux. For practical reasons we chose to measure CO_2 concentrations. Gas was pumped through a copper tube 2 mm in diameter, inserted in the soil to a depth of 0.5 m. It was sealed in glass tubes and later analysed by gas chromatography in the laboratory. The analytical uncertainty was 5% of the value.

Anomaly maps were constructed for SP, T and CO_2 by automatic interpolation using a kriging method. For SP and T (Figs. 4 and 5), gridding was performed using a 5-m square mesh. The interpolation of CO_2 (Fig. 6) is more difficult because the distribution of the data is less regular. We have dense data along seven profiles, 2.5 m apart, significantly larger than the data spacing along the profiles. Therefore, we used a different method of interpolation. Firstly, a generalized map of the entire area was interpolated with a wide mesh of 25 m, ten times

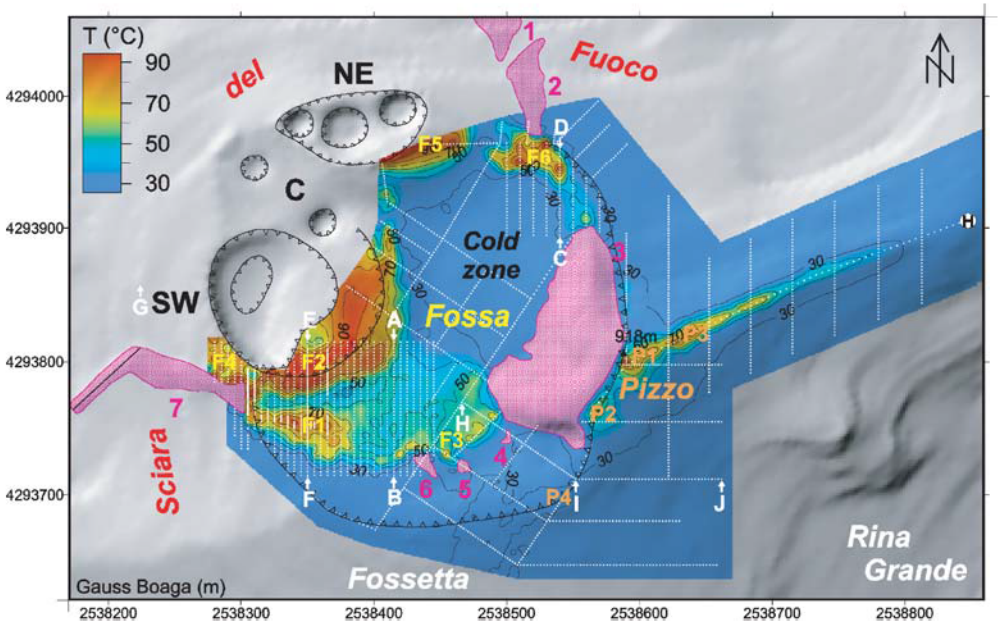

Fig. 4 Measured temperature (T) map (0.30 m below surface) of the summit area of Stromboli superimposed on a shaded relief map and volcano-structural features. *Black lines* are iso-temperature curves in °C. *White dots* are T measurement stations. *Numbers 1–7* are outcrops (*pink*) discussed in the text. *F1, F2, etc.* and *P1, P2, etc.* are anomalies and are discussed in the text. Other *symbols* are as in Fig. 2

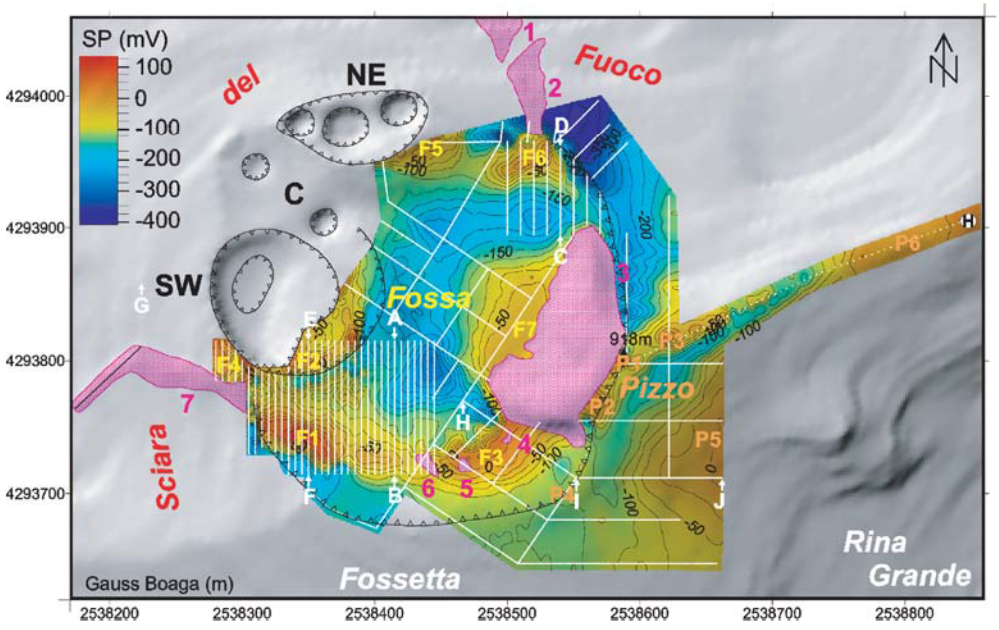

Fig. 5 SP map of the summit area of Stromboli superimposed on a shaded relief map and volcano-structural features. *Black lines* are iso-potential contours in mV. *White dots* are SP measurement stations. Other *symbols* as in Figs. 2 and 4

larger than the sampling spacing along the profiles, using both the data from this study and data from a wider survey (Finizola et al. 2002) where CO_2 data were acquired every 20 m along profiles shown on Fig. 6. A 5-m square mesh CO_2 map was then constructed using both the data along the profiles and the grid values of the large mesh map. Finally, areas not constrained by data have been blanked.

Gas sampling

Visible fumaroles on Stromboli volcano are located only very close to the active craters. Farther away, in the Fossa and Pizzo area, fumaroles were identified by T survey only. We sampled five fumaroles between September 1999 and August 2000: three in the Fossa area (F1–F3 in Fig. 4) and two in the Pizzo area (P1–P2 in Fig. 4). Dry gas samples were collected for isotopic composition analysis [$^3He/^4He$ and $\delta^{13}C(CO_2)$]. To correct for air contamination, all R/Ra values were corrected to the atmospheric contribution using the He/Ne ratio correction (Sano et al. 1982; Table 1).

We also tried to sample these fumaroles using the alkaline solution bottle method (Giggenbach 1975). Previously, only one NaOH sample has been obtained by Martini (1991) on the NE crater rim, at a temperature of 410 °C. However, this site is not safe most of the time because of volcanic activity, and cannot be considered a

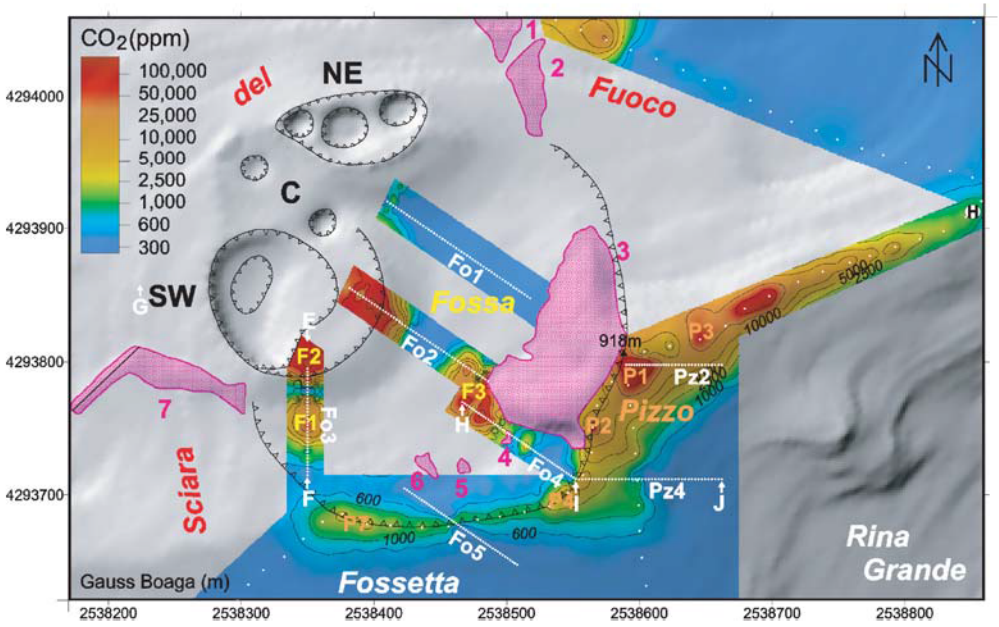

Fig. 6 Soil CO_2 map of the summit area of Stromboli superimposed on a shaded relief map and volcano-structural features. *Black lines* are isoconcentration curves in ppm. *White dots* are CO_2 measurement stations. Other *symbols* as in Figs. 2 and 4

Table 1 He and C Isotopic composition of the nine dry-gas samples collected in the Fossa and Pizzo areas above the maxima of T anomalies located in Fig. 3

Location	Anomaly	Date (day/month/year)	T (°C)	$4He/^{20}Ne$	$^3He/^4He$ R/Ra corr.	$\delta^{13}C(CO_2)$ ‰ vs. PDB
Pizzo	P1	02/09/99	88	2.04	2.84	n.d.
Pizzo	P2	02/09/99	62	n.d.	n.d.	–1.75
Fossa	F1	02/09/99	95	10.68	2.90	–2.01
Fossa	F2	02/09/99	98	n.d.	n.d.	–1.51
Pizzo	P1	28/04/00	88	0.49	1.88	–1.23
Fossa	F1	28/04/00	74	1.30	1.85	–1.87
Fossa	F3	28/04/00	59	n.d.	n.d.	–1.21
Pizzo	P1	31/08/00	88	0.70	2.46	–1.59
Fossa	F1	31/08/00	95	3.49	2.63	–1.94

Table 2 Chemical composition of total fluids for the four NaOH bottle samples collected at the F1 thermal anomaly (see Fig. 3) along the Fossa crater fault

Location	Anomaly	Date (day/month/year)	T (°C)	H_2O	CO_2	HF	HCl	Stot	He	H_2	O_2	N_2	CO	CH_4
				(μmol/mol)										
Fossa	F1	02/09/99	95	913,058	83,351	<d.l.	170	71	1.1	322	57	2,631	0.32	1.00
Fossa	F1	28/04/00	74	939,532	56,412	<d.l.	175	31	1.0	304	605	2,840	0.17	0.70
Fossa	F1	12/05/00	95	923,165	73,767	<d.l.	191	52	1.0	305	507	2,022	0.21	0.90
Fossa	F1	31/08/00	95	936,255	56,781	<d.l.	166	40	1.6	259	885	5,273	0.16	0.79

practical sampling site for geochemical monitoring. We tried to use this sampling technique at the fumaroles in the Fossa and Pizzo areas. The measurements were successful only at F1, where there was low atmospheric contamination. F1, nowadays only detectable by geophysical or geochemical measurements, was described by Bullard (1954) from photographs taken in June 1952 as an elongated fumarolic area with cracks. Between September 1999 and August 2000, four samples were collected using this sampling technique at a reference point located precisely at the maximum temperature of 95 °C in the F1 anomaly. However, at the end of May 2000, we were unable to collect a sufficient quantity of condensate due to higher air contamination at the sampling site. This difficulty may arise from variations in the atmospheric pressure, variations in the volcanic activity or from technical sampling problems. The results are presented in Table 2.

For soil gas sampling, a metallic tube was inserted to 50 cm depth in the ground. To collect dry gas, we used a three-way valve. Fumarolic gases were first pumped into a syringe and injected into a 50-ml Pyrex bottle with two stopcocks. Total fluids were collected by connecting a 150-ml Pyrex bottle containing 50 ml of NaOH 4 N to the tube (the bottle has two stopcocks in Teflon and air has been evacuated). Pressure differences caused fumarolic

gases to enter the bottle, but vapour condensates and acid gases (CO_2, HCl, HF, H_2S, SO_2) were absorbed in the NaOH solution by acid–base reaction. Unabsorbed gases (He, H_2, CO, CH_4, O_2, N_2) were collected in the head space.

Temperature, SP and CO_2 maps and anomaly identification

Temperature map (Fig. 4)

At the summit of Stromboli, fumaroles are only present close to the rims of the active vents. The rest of the hydrothermal system is a typical sub-fumarolic system where steam condenses just below the ground surface by atmospheric cooling (Aubert et al. 1984). Therefore the exploration of the hydrothermal system requires the use of geophysical or geochemical techniques. There have been several previous successful surveys aimed at detecting upward flow of hot fluids using shallow temperature measurements (e.g. Ballestracci 1982a; Nishida and Tomiya 1987; Aubert and Baubron 1988; Matsushima et al. 1990; Aubert 1999). The temperature map of the summit of Stromboli (Fig. 4) displays several thermal anomalies in the Pizzo, Fossa and active crater zones.

The Fossa and active crater area

Six temperature anomalies, F1–F6 (Fig. 4), are recognized in the Fossa craters area. F2 and F5 are close to the rims of the SW and NE craters respectively, with maximum temperatures between 98 and 99 °C. The maximum of the F2 anomaly is within the SW crater, although the temperature reaches 90 °C outside the rim. The temperature decreases to 60 °C near the active vent. F1 and F6 anomalies have temperature maxima between 94 and 96 °C. The F1 anomaly is elongated parallel to the line linking pyroclastite outcrops 6 and 7, and is connected to F3 by a zone of moderate amplitude anomaly. The F6 anomaly has four distinct maxima; three of them between 94 and 96 °C and the 4th at 58 °C. The anomaly is slightly curved and spreads between pyroclastite outcrops 2 and 3. The F4 anomaly reaches a maximum of 92 °C and is located close to the SW crater rim, at the headwall of the Sciara del Fuoco. F3 is a complex anomaly with four distinct maxima between 68 and 73 °C. They are located approximately 10–15 m north-west of the pyroclastite outcrops 4, 5 and 6. Locations of profiles in this area were chosen to cross temperature maxima found at approximately 10 cm depth by instantaneous infrared temperature measurements. The centre of the Fossa, surrounded by the above described anomalies, is characterized by the absence of temperature anomalies.

The Pizzo area

Three temperature maxima (P1–P3, Fig. 4), from 70 to 87 °C, are distinguished in the Pizzo area. They coincide with hydrothermally altered rocks observed at the surface along the crest between the helicopter pad and the summit (the alteration is particularly characterized by gypsum deposits). These anomalies are very narrow, with the temperature decreasing rapidly outward to normal values. A weak but significant anomaly (P4) is also present along the SW Pizzo crest. A similar slight T anomaly is also present in the northern part of P1 anomaly, along the eastern side of pyroclastic outcrop 3.

SP map (Fig. 5)

There are more SP than temperature anomalies, and both positive and negative SP anomalies are found. Most of the positive anomalies are associated with temperature anomalies, but some are not.

Positive SP anomalies associated with temperature anomalies

All temperature anomalies are associated with positive SP anomalies, although the shape of the two types of anomaly may differ significantly and the location of their respective maxima may not be identical. Along the seemingly curvilinear line of anomalies F1, F3 and F6, for F6, the maxima of temperature and SP anomalies nearly coincide (Fig. 7B), but for F1 and F3, the correlation is more complex (Figs. 7A and 8). This will be examined in more detail in the analysis section. Near the active craters, SP and T anomalies are present concurrently at F4, F2 and F5. Along the Pizzo crest, SP highs are associated with temperature anomalies P1–P4.

Positive SP anomalies without a T anomaly

Three positive SP anomalies are not associated with temperature anomalies. Anomaly F7 occupies the eastern part of the Fossa area and apparently extends, at least partly, over the large unmapped outcrop of the Pizzo pyroclastites. P5 and P6 anomalies are located east of the Pizzo area. All three anomalies have a longer wavelength than other summit anomalies.

SP minima

At the margin of the survey, negative SP anomalies are present north-east of F5 and F6 and south-west of F1. Only the SP low, north-east of F6, is well mapped. The bottom of the Fossa is a zone of SP lows surrounded by positive SP anomalies F1, F2, F3, F5, F6 and F7. In the Pizzo area, a band of SP lows parallels the positive

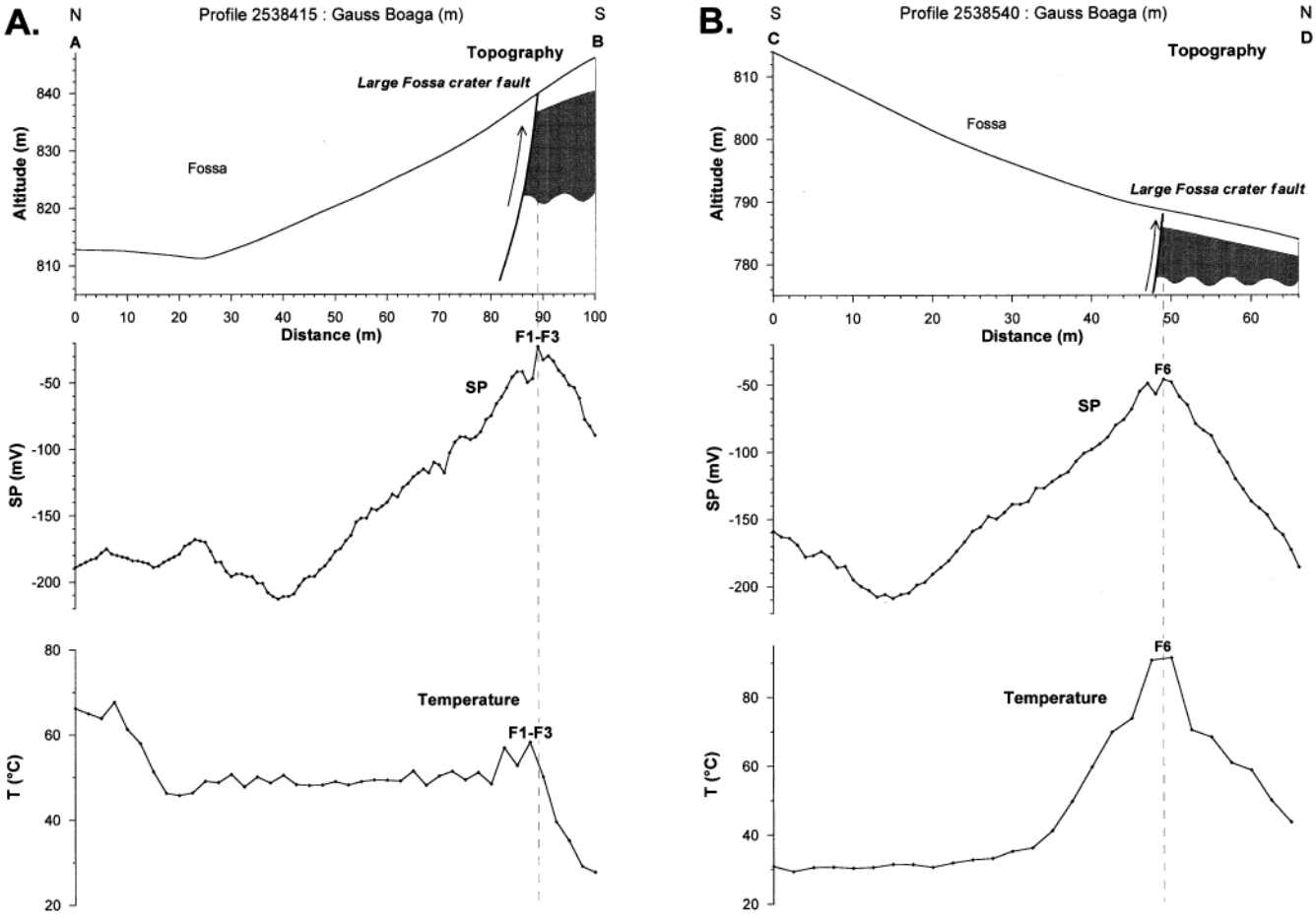

Fig. 7 **A** T, SP and topographical A–B profile in the detailed study area shown in Fig. 2. The name of the profile corresponds to the easting co-ordinates. *F1, F3, etc.* correspond to the anomalies shown on the maps. Inferred faults are represented by *solid and discontinous lines*. The *arrows* show the inferred fluid circulation along the faults. *Grey shading* represents contrasting lithology across the faults. **B** Same symbols as Fig. 6A. The C–D profile, located east of the NE active crater, is shown in Fig. 2

anomalies P1, P2 and P3 and follows the arcuate topography of the headwall of the Rina Grande depression.

CO_2 map (Fig. 6)

This map is constructed from fewer data than the other maps and, thus, its interpolation is less well constrained, but it shows a good correlation with the temperature map particularly.

The Fossa area

The profiles measured in the Fossa area show that anomalies F1–F3 are characterized by huge CO_2 concentrations, reaching values close to 100,000 ppm. One surprising result is the virtual absence of CO_2 emanations (i.e. atmospheric concentrations are observed) very close to the active craters in some areas. Another particularity of this zone with respect to the temperature map (Fig. 4), is the presence of high CO_2 values (between 1,000 and 3,000 ppm) along the crest between the Fossa and Fossetta areas (P7 anomaly in Fig. 6).

The Pizzo area

In the Pizzo area, anomalies P1–P3 are also characterized by high CO_2 concentrations, up to 50,000 ppm, whilst anomaly P4 has a concentration of about 6,000–10,000 ppm. A smaller, but significant band links P4 and P7 along the topographic crest between the Fossa and Fossetta areas. Along this crest, only a CO_2 anomaly is observed (values of 1,000–4,000 ppm). This fact strongly suggests that CO_2 measurements are more sensitive to hydrothermal circulations than SP and T measurements.

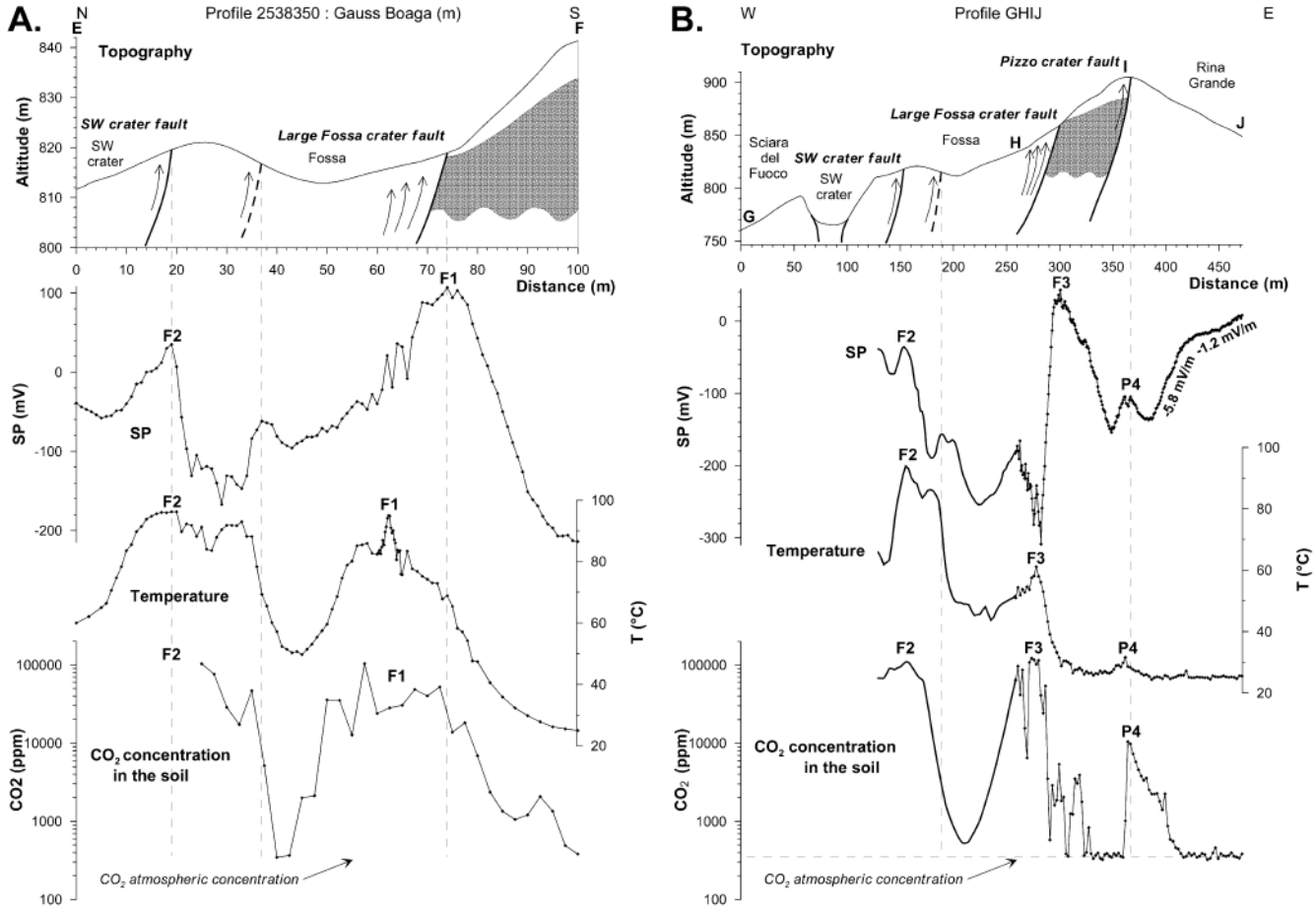

Fig. 8 **A** CO_2, T, SP and topographical E–F profile located in the detailed study area shown in Fig. 2. The name of the profile corresponds to the easting co-ordinates. *F1, F2, etc.* correspond to the anomalies shown on the maps. **B** *GHIJ* profile shown in Fig. 2 including Fo4 (HI) and Pz4 (IJ) profiles. Between *G* and *H*, measurements are interpolated on the CO_2, T and SP maps. The same symbols are used as in Fig. 6A

Analysis of T, SP and CO_2 correlations. Fluids geochemistry

Correlations between T and SP maxima

Analysis of the maps and profiles shows that the correlation between SP and T anomalies is direct (i.e. the anomalies are nearly coincident in their location and extent) in some cases and more complex in others. Anomalies F5 and F6 in the Fossa area (Figs. 4, 5 and 7B) and anomalies P1–P4 in the Pizzo area (Figs. 4, 5 and 8B) exhibit a direct correlation between SP and T. For anomalies F1 and F2 (Fig. 8), SP and T anomalies are only partly superimposed, the T anomaly being wider on the Fossa side in both cases. In F3 (Fig. 8B), we have one 50–60-m wide T anomaly and two SP anomalies. The maximum of the largest SP anomaly is located about 20 m SE of the T maximum. This 40–50-m wide anomaly has a high amplitude (~350 mV) and a sharper gradient on the Fossa side. The secondary SP anomaly (~100 mV) coincides with the NW part of the T anomaly.

Correlation between short wavelength SP minima and T maxima

The absence of visible fumarolic areas, excepted near the active vents, and the presence of high thermal anomalies at the surface suggest that steam water rising in the hydrothermal system condenses at shallow depths. Accordingly, the temperature maxima probably correspond to the top of rising cells in the convective hydrothermal system. On the other hand, SP may reflect fluid flow in different directions, and the SP minima may be associated with downward and/or lateral flow of condensed water. For this reason, special attention has been paid to short wavelength negative SP anomalies that could be associated with shallow water movement.

The high signal to noise ratio of data within the Fossa clearly shows short wavelength anomalies superimposed on larger scale features (Fig. 9). In the detailed study area (Fig. 2), very dense SP coverage (data spacing of 1 m along profiles 5 m apart) means that short wavelength anomalies can be correlated between the profiles with good reliability. Figure 10 shows that short wavelength

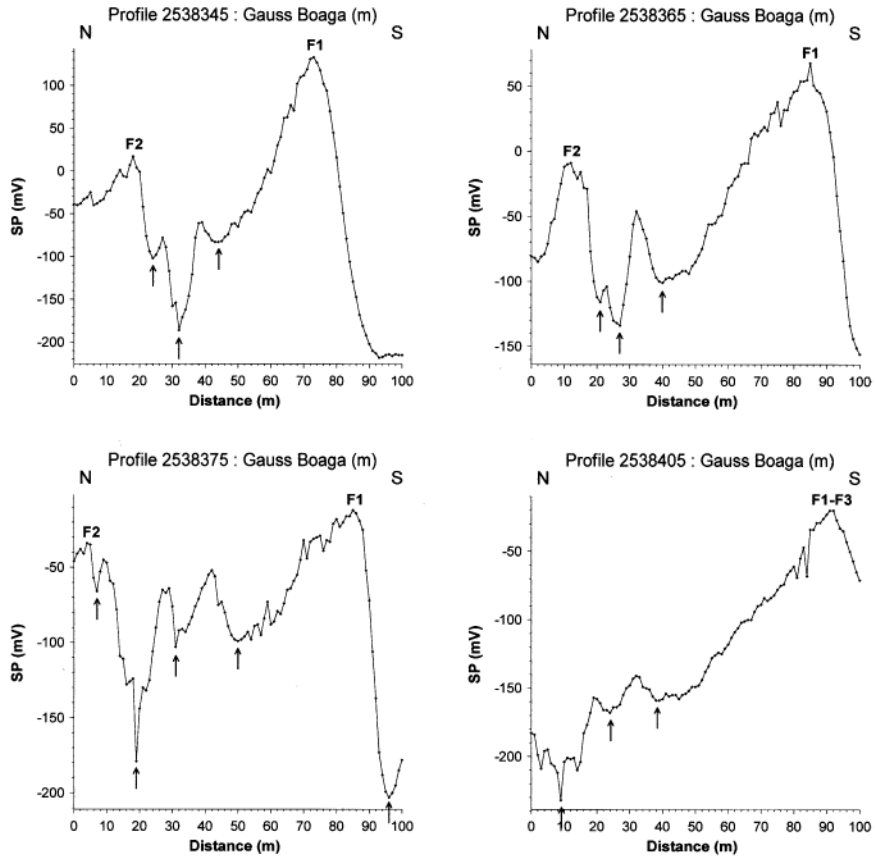

Fig. 9 SP N–S profiles located in the detailed study area shown in Fig. 2. The *arrows* show the SP minima plotted in Figs. 10 and 14. The name of the profile corresponds to the easting coordinates. *F1, F3, etc.* correspond to anomalies located on the maps

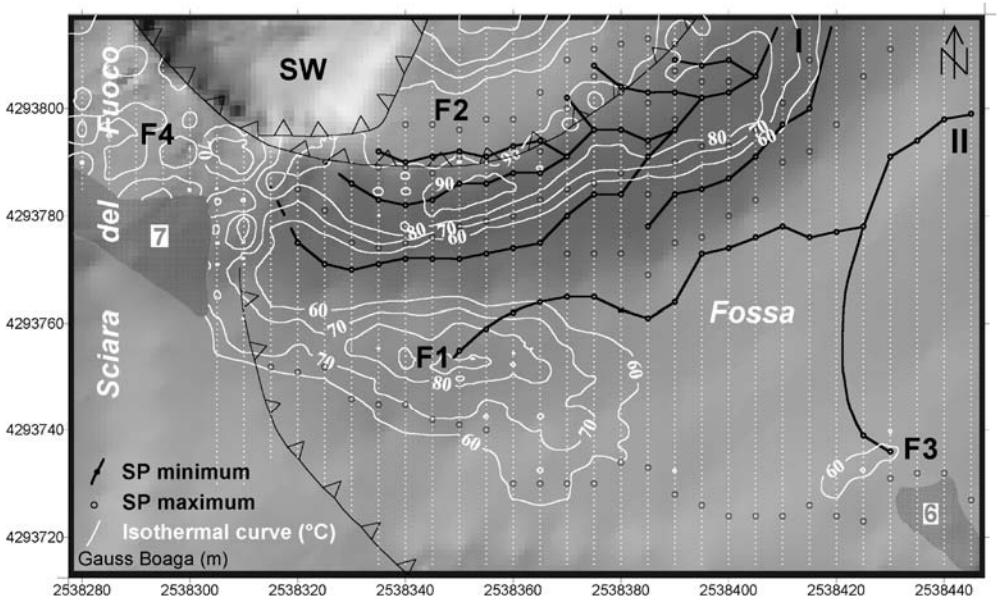

Fig. 10 Map showing locations of the SP maxima and minima and the isothermal curves (in °C) superimposed on a shaded relief map and volcano-structural features of the detailed study area (shown in Fig. 2). *White dots* SP measurement stations. Numbers *6* and *7* are outcrops shown in Figs. 2, 3, 4 and 5. *F1, F2, etc.* are Fossa T anomalies. *I* and *II* correspond to the main axes of the SP minima network

SP lows are organized in a drainage-like network diverging from the main thermal anomalies F1 and F2.

In the Pizzo area, the six E–W profiles (Pz1–Pz6; Fig. 2) on the east flank display a different SP style from the Fossa area (Figs. 5 and 8B). There is no succession of short wavelength anomalies, but a steady decrease in SP from east to west, as far as positive anomalies P1–P4, which correlate well with T anomalies. Thus, we have a band of minima on the east of the latter anomalies. When SP values are plotted against station elevation, there is a linear relationship between the two parameters for the eastern descending part of the profiles. Such negative SP/

altitude gradients (e.g. 5.8 and 1.2 mV/m for Pz4 profile in Fig. 8B) clearly resemble purely hydrogeologic gradients.

T and CO_2 correlation

A remarkable feature of the survey is the strong correlation between T and CO_2 anomalies. Along the profiles (Fig. 8), the CO_2 anomalies seem to mimic the T anomalies. There are, however, some differences between the two signals. Generally speaking, the CO_2 profiles are not as smooth as the temperature profiles. One reason may be that CO_2 at shallow depth (0.5 m) can be perturbed locally by atmospheric dilution in the highly permeable surface layers (as suggested for NaOH bottle sampling), whereas atmospheric cooling of thermal anomalies at 0.3-m depth is more dilute or homogeneous, and can also be smoothed by thermal conductivity. The correlation between T and CO_2 is quantified in Fig. 11. Figure 11A shows the overall correlation between the two parameters as well as its large dispersion. The scatter could be due to two types of effects.

1. As mentioned above, shallow dilution processes by atmospheric air tend to shift CO_2 and T values toward that of the air (~330 ppm, 25 °C).
2. In addition, thermal conduction is probably significant in some areas, indeed, as implicit in the conclusion that SP, T and CO_2 anomalies are generated by convective circulation of heat and fluids. However, especially near the active vents, where the heat supply is sustained and large, a large conductive flux component of heat is expected. As a result, the T values will be increased by the conductive flux whereas the CO_2 values remain unaffected. This is what is observed in Fig. 11A where the data have been sorted into three groups depending on their distance from the active craters. It is obvious that the correlation between CO_2 and T becomes better as we go farther from the active craters. In the lower part of Fig. 11A, where CO_2 remains near atmospheric CO_2 concentrations, the temperature variations may be inferred to be governed by heat conduction only. Conversely, in the colder Pizzo area, CO_2 and T are highly correlated as shown in the enlarged diagram of Fig. 11B.

T and amplitude variation of high frequency SP signal

Whereas most of the profiles are characterized by an excellent T and SP signal/noise ratio, there is a significant increase in the amplitude of high frequency (HF) SP signal in a few places. This is so in the F4 anomaly area (Figs. 4 and 5) and locally in some parts of the profiles (see for example Figs. 8 and 9).

Figure 12 is a map of the amplitude of HF SP signal. This was calculated for each profile (except the Pz1 profile where the data spacing is wider than the 1-m spacing of other profiles) by subtracting a smoothed profile (three points running average) from the raw profile. Absolute values were interpolated (2-m square mesh) to construct the map presented.

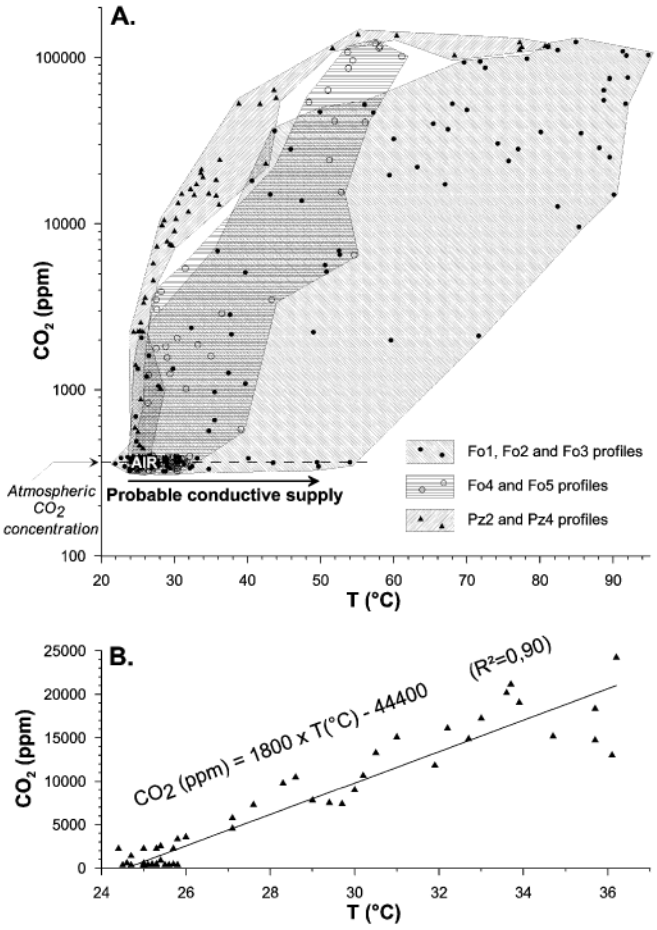

Fig. 11 **A** Graph of CO_2 versus T for the area near the active craters shown in Fig. 2. **B** Detail CO_2 versus T graph for the Pizzo area, corresponding to profiles Pz2 and Pz4 shown in Fig. 2

The map of the amplitude of HF SP signal (Fig. 12) reveals that high levels of HF signal are closely associated with T anomalies (Fig. 4). It is also clear that the slight 10–20-m offset between T and SP highs over the F1 and F3 anomalies is not observed between HF SP signal and T anomalies. In addition, the high amplitude HF SP signal is present in two areas where T anomalies were not detected: the northern part of anomaly P1 and the southern part of anomaly F4. The understanding of the physical processes generating these anomalies is beyond the scope of this work, but the empirical relationship between high amplitude HF SP signal and the T anomalies suggests that HF SP signal could help to detect subsurface thermal anomalies in some cases.

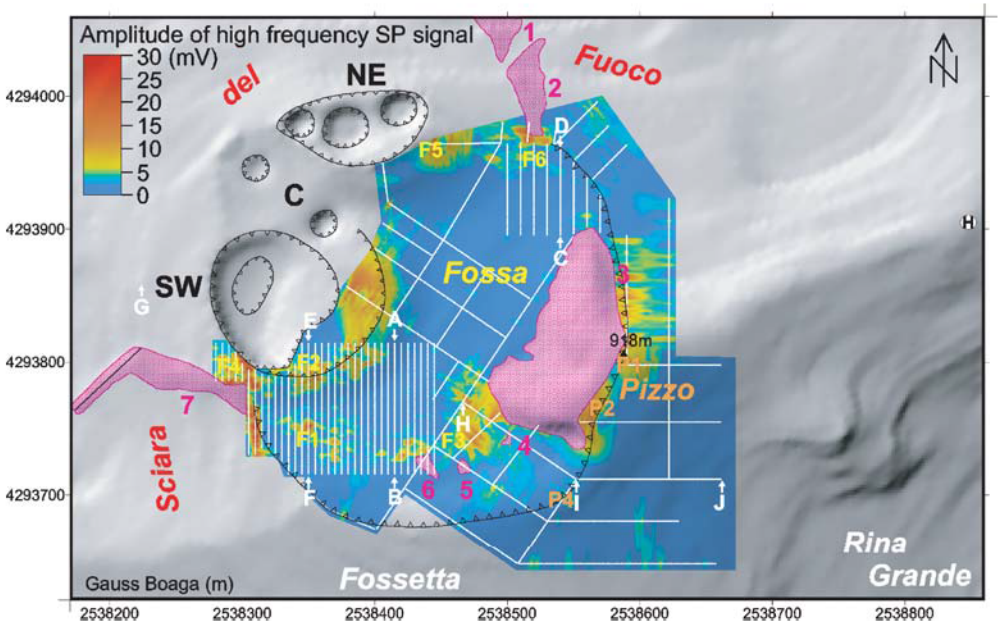

Fig. 12 Map of the amplitude of high frequency SP signal in the summit area of Stromboli superimposed on a shaded relief map and volcano-structural features. *Black lines* correspond to iso-potential curves in mV. *White dots* SP measurement stations. *Numbers 1–7* are as in Figs. 3, 4 and 5. *F1, F2, etc.* and *P1, P2, etc.* are Fossa and Pizzo SP noise anomalies discussed in the text. Other *symbols* as in Fig. 2

Interpretation

Large positive anomalies of SP, temperature and CO_2 emanation are observed at the summit of Stromboli and indicate intense hydrothermal activity. The very dense multi-parameter data coverage allows interpretation of summit features at a scale unrivalled in previous works. We will focus on the structural interpretation of the central area of Stromboli and on the study of its hydrothermal activity.

Relationship between structural boundaries and anomalies

Arguments for a circular Pizzo crater and nested craters

The Fossa depression is surrounded by a quasi continuous belt of positive SP anomalies and by a similar belt of temperature anomalies, interrupted at F7 (Figs. 4 and 5). Where available, CO_2 data show the presence of significant anomalies concurrent with temperature anomalies (Fig. 6). One group of anomalies (F2, F4 and F5) is directly associated with the active vents. The curved line of anomalies formed by F1 and F3 is nearly parallel to, and about 50 m away from, the rim of the Pizzo crater. The other curved line of anomalies, from F6 to the outcrop of the Pizzo pyroclastites, is also practically parallel to, and about 15 m away from, the continuation of the Pizzo crater rim. The latter can be inferred in this area from the analysis of air photos (Fig. 13) and from the topography that exhibits a smooth but conspicuous crest line. Between these two segments of curved lines of anomalies lies the large outcrop of the Pizzo pyroclastites. The latter are inferred to belong to a tuff cone formed during the first stage of the recent Stromboli cycle (Hornig-Kjarsgaard et al. 1993; Keller et al. 1993), ca.

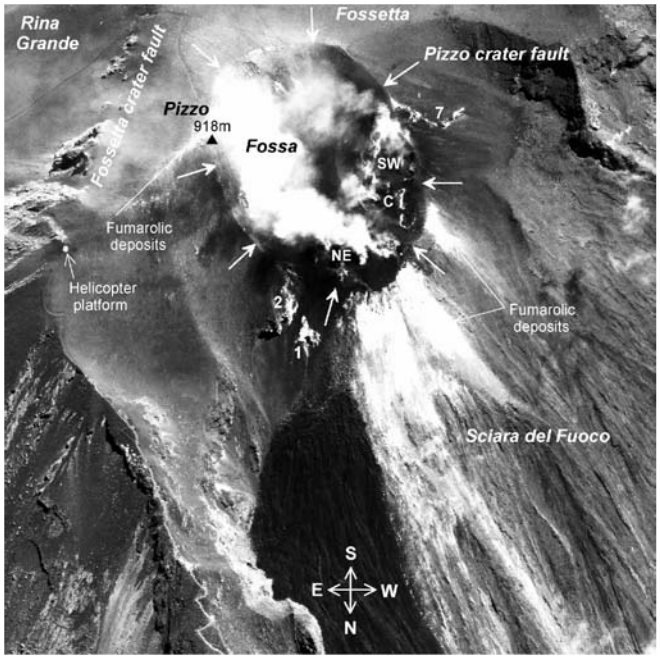

Fig. 13 Aerial photograph of the summit area of Stromboli showing the circular nature of the Pizzo crater

5,000 years B.P. (Gillot 1984; Gillot and Keller 1993), and have apparently been impounded by the Pizzo rim to the east. This large outcrop is thus buttressed by the wall of the Pizzo. The Pizzo pyroclastites must unquestionably have had a larger extent after their eruption, and smaller outcrops of pyroclastites are observed in several places as shown on the various maps presented in this work, and also at a shallow depth between Pizzo and the helicopter pad. These could be related to an explosive cycle, but none of them forms a topographic feature comparable

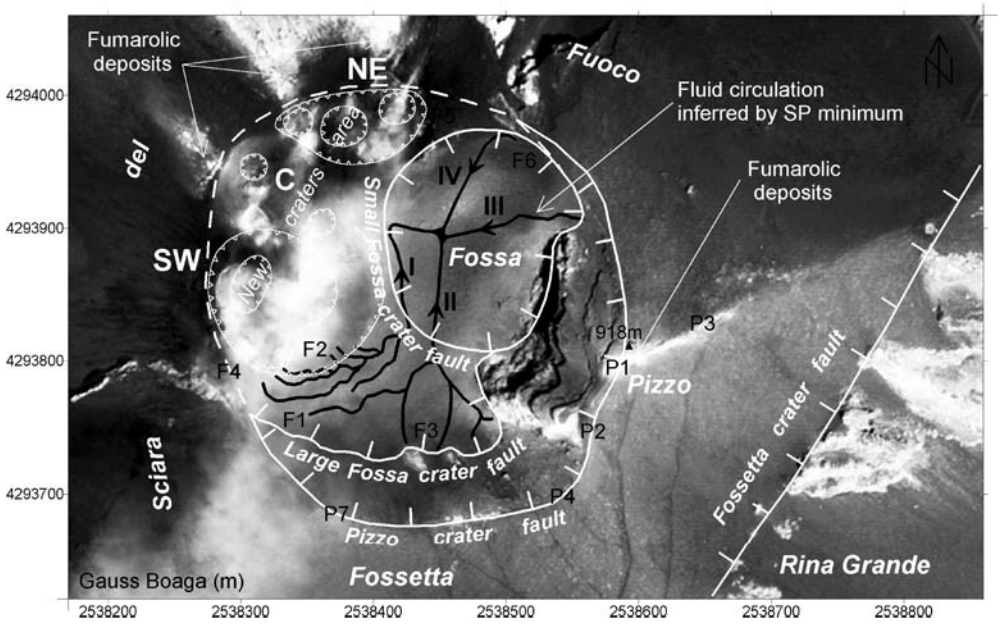

Fig. 14 Map of the volcano-structural features inferred from T, SP and CO_2 surveys superimposed on an air photo (courtesy of Klaus Gwinner, DLR—German Aerospace Center image; Gwinner et al. 2000). *Black lines* show inferred shallow water circulation (short wavelength SP minima) diverging from T anomalies and flowing toward the Small Fossa crater. *I*, *II*, *III* and *IV* correspond to the main axes of water circulation. *F1, F2, etc.* and *P1, P2, etc.* are the Fossa and Pizzo thermal anomalies, respectively. Other *symbols* as Fig. 2

with the large Pizzo outcrop. The absence of a similar accumulation of pyroclastites on the southern rim of the Pizzo crater, and the fact that the Pizzo outcrop ends abruptly to the south, suggest that subsequent events have dismembered the pyroclastite ring. Erosion alone cannot be held responsible for the missing parts of the Pizzo pyroclastites to the south, so volcanic or volcano-tectonic processes could be responsible for the present-day morphology and extent of the Pizzo pyroclastites. Outcrops 4, 5 and 6 are located at a short distance from the Pizzo outcrop, but their highest point is about 50 m lower in altitude than the top of the Pizzo outcrop. This strongly suggests that they have slid along the Pizzo crater fault and that, therefore, the F1–F3 anomalies are located above a zone of collapsed pyroclastite deposits.

These observations, together with the distribution of the various anomalies (Figs. 4, 5 and 6) and the analysis of air photos (Fig. 13) and topography (e.g. Fig. 2), lead us to define a new structural framework for the summit of Stromboli. In this framework, the Pizzo is not a depression opening towards the Sciara del Fuoco (Keller et al. 1993, in Fig. 2; Tibaldi 2001), but truly a central crater with smaller nested craters inside (Figs. 14 and 15).

The boundaries of the Pizzo crater can be recognized on the basis of (1) the anomalies described here, (2) the dipping of the deposits (Tibaldi 2001), (3) topographic evidence and/or (4) air photo analysis, depending on the area. The eastern and southern limits are obvious from the topography. The eastern limit is also marked by the easterly border of the Pizzo pyroclastites outcrop and by anomalies P1, P2 and P4 (and probably north of P1, where a weak T anomaly, similar to P4 in amplitude, is present along the Pizzo pyroclastites). The southern border is also coincident with the P4–P7 line of CO_2 anomalies. The identification of the northern and western boundaries relies mostly on topographic and air photo evidence

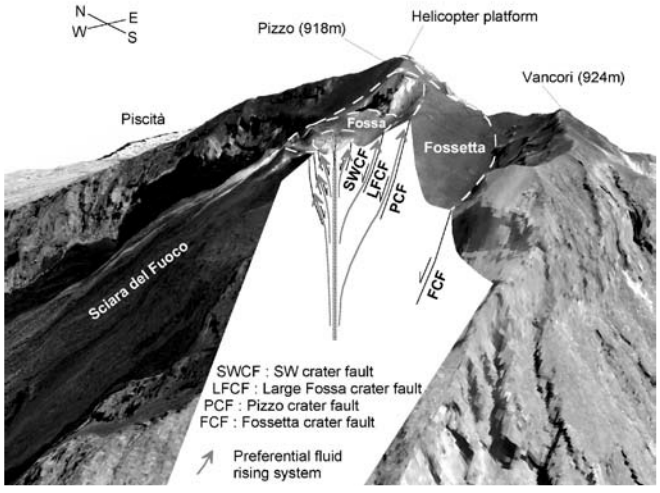

Fig. 15 Oblique representation of the upper part of Stromboli island (derived from the superimposition of an airborne image (courtesy from Klaus Gwinner, DLR—German Aerospace Center image; Gwinner et al. 2000, on a DEM). The different volcano-structural features and preferential fluid circulations inferred from SP, T and CO_2 surveys are show on the view and in section. Other *symbols* as in Fig. 2

because these areas are not covered by our survey. The air photos (Figs. 13 and 14) show a set of hydrothermally altered patches or fumarolic deposits to the north of the NE crater and to the NW of the central crater. These patches lie outside of the inferred limit of the Pizzo crater and abruptly stop at its limit.

Based on this evidence, the Pizzo crater is shown in Figs. 14 and 15 and is clearly visible in oblique air photo (Fig. 13). Inside this main central crater are located the presently active craters and a complex of concealed craters that can only be located using our new data. The SW, central and NE active craters are situated near the N

and NW borders of the Pizzo crater, which is in the direction of the Sciara del Fuoco. Although this zone is not covered by our survey, F2 and F4 appear to be associated with faults concentric to the SW crater (Fig. 8), and F5 with the NE crater. The concealed craters that we infer are nested in the eastern and southern part of the Pizzo crater. We demonstrate below how this interpretation is supported by the data.

The SP anomaly F3 coincides with the outcrops 4, 5 and 6 of the Pizzo pyroclastites, whereas the corresponding temperature and CO_2 anomalies are slightly shifted to the NW. The curved line of anomalies F3 to F1 coincides with the Pizzo crater rim at the western end of F1. At this location, there is no SP or T evidence for the continuation of anomaly F1 outside the Pizzo crater rim in the Sciara del Fuoco area. In other words, the extension of anomaly F1 seems to be constrained by the Pizzo crater rim. On the opposite side of the Fossa area, another curved line (F6 anomaly) seems to be also constrained inside the Pizzo crater rim. The western border of the Pizzo pyroclastites, between F3 and F6, corresponds to a steep wall. Tibaldi (2001) suggests that this morphology results from a sector collapse crossing the Fossa area. Anomalies F1, F3 and F6 fit in with the hypothesis of a fault crossing the western border of the Pizzo pyroclastites, but the horizontal trace of the inferred fault does not fit with that of a wide angle fault open toward the Sciara del Fuoco, but with that of a circular structure nested in the Pizzo crater. We propose that this fault corresponds to a crater, herein called the Large Fossa crater (Figs. 14 and 15).

The postulation of the presence of this crater led us to examine in more detail the data along the profiles. As noted earlier (Correlations between T and SP maxima Section), the shape of the SP and T anomalies in F1 and F3 are not exactly similar and their maxima are not co-located. However, the proposed interpretation implies that the inferred Large Fossa crater fault constitutes a permeable zone allowing the escape of hot fluids and gas from the hydrothermal system. The source of the anomalies, therefore, is common to the SP, T and CO_2 parameters. The explanation of the differences in the shape of the anomalies can probably be explained if we examine the physics of the generation of the anomalies. We can reasonably assume that we have contact terrains with contrasting physical properties: the Pizzo pyroclastites, the highly permeable fault zone and the subsequent filling of the Fossa by collapsed brecciated blocks and/or tephra. Sill (1983) has demonstrated that, for a given source, the shape, position and amplitude of the associated anomalies can vary to a large extent, depending upon the contrasts in physical properties of the ground that influence the SP signals (electrical resistivity, permeability, coupling coefficients). The same analysis applies to thermal convection and conduction and to circulation of CO_2, T and CO_2 anomaly geometry with amplitude being also dependant upon the properties of the rocks. It is, therefore, logical to assume that adjacent rock types with contrasting physical properties in the fault zone will result in complex anomaly geometries for the different parameters. Quantifying this qualitative explanation would require complex modelling of the different signals and a good knowledge of the physical parameters involved, clearly beyond the scope of this work. Therefore, we assume that, to a first approximation, a single hydrothermal circulation gives rise to the anomalies observed along the presumed concealed fault extending from F1 to F3. Using the same rationale for the continuation of the Large Fossa crater fault to anomaly F6, the difference in shape between the SP and temperature anomalies (Fig. 7B) is not so pronounced, probably because the contrasts in the physical properties of the formations around the fault are different from those in the vicinity of F1 and F3.

A striking feature inside the large Fossa crater is the more or less circular 'cold zone' (Fig. 4), with virtually no temperature anomaly and no SP signal comparable with the anomalies discussed above. CO_2 profile Fo1 (Fig. 6) in this area shows only atmospheric concentrations. SP anomaly F7, on the Fossa border of the Pizzo pyroclastites block, has a significantly longer wavelength, suggesting a deeper source. Obviously, the 'cold zone' is a distinct structure of the Fossa. The characteristics of this area are similar to the Vulcano craters. Indeed, a detailed SP and T survey of Vulcano by Chébli (1997) shows that the floor of the recent craters of Vulcano contain similar 'cold zones', whereas large T anomalies (ca. 100 °C) are present at the periphery of the crater bottoms. This is interpreted as the filling of the craters by highly impermeable products. Fluids and heat can only escape along the border faults of the craters. The same interpretation can be applied to the 'cold zone' of the Fossa. It would be otherwise difficult to explain the absence of thermal, CO_2 and SP anomalies in an area close to the highly active craters and to major T, SP and CO_2 anomalies. We name this 'cold zone' the Small Fossa crater. It is highly probable that this crater and the Large Fossa crater are the source of the Pizzo pyroclastites. Indeed, the products of the Pizzo block have been recognized as proximal facies (Hornig-Kjarsgaard et al. 1993) and dip toward the 'cold zone'.

In summary, our new structural interpretation of the summit area of Stromboli leads to the following sequence of events (Fig. 15):

1. After the Fossetta crater formation, which marks the transition from NeoStromboli to Recent Stromboli cycles (ca. 5,000 years B.P.), a large circular crater about 350 m in diameter, the Pizzo crater, formed.
2. A complex of nested craters later opened within the Pizzo crater. It comprises the Large and the Small Fossa craters, respectively about 280 and 150 m in diameter. It is not established whether or not they constitute two units of a single structure, although this is very likely. They appear to be the source of the Pizzo pyroclastites.
3. Collapses of the Pizzo pyroclastites into the Fossa craters occurred along parts of the crater rims, during

or immediately after the eruption of the Pizzo pyroclastites.
4. The Small Fossa crater filled with impermeable material.
5. The presently active crater complex formed recently.

This model is consistent with the different observations and has major implications for the mechanisms of fluid and heat transport in the summit area of Stromboli:

1. Crater faults are the preferential outlets for hydrothermal circulation.
2. The inferred Small Fossa crater infill and the Pizzo pyroclastites are impermeable and block the upward hydrothermal circulation.

Shallow fluid circulation in the Fossa area revealed by short wavelength SP signals

In the Pizzo and Fossa areas, the absence of visible fumaroles strongly suggests that the T anomalies lie at the head of underlying convective cells. Figure 10 shows that short wavelength SP lows in the detailed survey area are organized in drainage-like networks diverging from the main thermal anomalies F1 and F2. The same is true of the entire Fossa area (Fig. 14). It appears that the resulting pattern is compatible with the condensation of water at T anomalies F1, F2, F3, F5 and F6, and the subsequent subsurface downhill flow of condensed water in the direction of topographic lows. This very shallow water circulation in the Fossa area is apparently organized along four main axes (I, II, III and IV in Fig. 14). It converges in the middle of the Small Fossa crater, which, as shown above, is underlain by highly impermeable layers. There is, therefore, a possibility that a perched water body can exist at shallow depth beneath the Small Fossa crater. The presence of a water reservoir close to the active craters (less than 100 m) unquestionably represents a major hazard because its interaction with a magma intrusion would result in strong phreatic and phreatomagmatic explosions. Indeed, the strongest historical paroxysm event, on 11 September 1930 (Rittmann 1931), began with two strong phreatic explosions. Therefore, possible water accumulation close to the active craters deserves special attention in risk evaluation at Stromboli.

The SP lows at the east of the Pizzo area, near the head of the Rina Grande flank collapse, can tentatively be interpreted as downward flow of water condensed at T anomalies P1–P4. However, in this sector, water is evacuated away from the active craters and poses less threat.

Fluid geochemistry

SP, T and CO_2 surveys show two distinct fumarolic areas (the Pizzo and Fossa areas) separated by the structural limit of the Large Fossa crater (Fig. 14). To determine if the fluids have a common origin in these two areas, we collected dry gas samples for isotopic composition [R/Ra and $\delta^{13}C(CO_2)$] three times in one year (Table 1). Our data range from 1.85 to 2.90 for R/Ra and from −1.21 to −2.01 for $\delta^{13}C(CO_2)$, in good agreement with the data presented by Carapezza and Federico (2000). At the same time, similar R/Ra ratios were observed in both the Pizzo and Fossa areas and $\delta^{13}C(CO_2)$ values also appear to be very similar with a very slightly higher magmatic contribution in the Fossa area. Moreover, these values fluctuate similarly in time for the two fumarolic areas, suggesting a common origin for the fluids rising in the Pizzo and Fossa areas and indicating that the structural limit of the large Fossa crater does not act as a fluid barrier for fluids rising along the Large Fossa crater and Pizzo crater faults. However, the latter exhibits a higher air contamination (lower He/Ne ratio; Table 1), precluding the use of the alkaline bottle sampling technique. Only anomaly F1, located along the Large Fossa crater fault, allows total fluid sampling because the air contamination is very low. This anomaly has water concentrations of between 91 and 97% of total fluids and a very low concentration in acid gases (HCl, HF, Stot; see Table 2). Therefore, anomaly F1 appears to be the best point for future geochemical monitoring on Stromboli Volcano.

Discussion

In a previous study (Finizola et al. 2002), the results of a SP and CO_2 survey at the scale of the island of Stromboli were described. It is important to compare the observations at the scale of the island with that of the present study focused on the active summit area.

The island-wide survey was carried out with SP and CO_2 measurements every 20 m along six radial profiles extending from the summit to the sea. A common finding of the two surveys is that the distribution of the anomalies is greatly influenced by the presence of structural limits, such as crater, caldera or landslide faults. These discontinuities clearly constitute permeable drains on Stromboli. However, the phenomena observed at these limits varies in the different zones. In the summit area, the present work shows the co-occurrence of SP, T and CO_2 positive anomalies above the main faults. The transfer of hot hydrothermal fluids, heat and gases around the active area, thus, is controlled by the presence of more permeable paths along the faults. In contrast, further from the active area, an inverse relationship was found between SP and CO_2 anomalies in the island-wide survey. High CO_2 emanations were correlated with significant negative SP anomalies. This may be explained if we consider that the permeable faults away from the active zone still allow the upward migration of deep CO_2 degassing, but that, as these zones are not affected by shallow thermal anomalies, and therefore by shallow hydrothermal convection cells, they promote the downward migration of ground water.

From the island-wide survey it was concluded that a large hydrothermal zone occupies much of the summit of Stromboli. This hydrothermal zone appears to be constrained by the PalaeoStromboli I (PST I) and PST III caldera faults (Fig. 1). Of course, this large hydrothermal system does not show the prominent surface evidence of the Pizzo–Fossa zone and represents probably a deeper intra-edifice system that can be recognized only through geophysical and geochemical measurements. The Pizzo–Fossa shallow hydrothermal system studied in the present work is located inside the large hydrothermal zone of Stromboli (Fig. 1).

Conclusion

The uniqueness of the work presented here lies in the very dense data coverage achieved near the active area of an active volcano. To our knowledge such a survey has never been carried out before in a similar context. The high density of data, the diversity of the measured parameters and the accuracy of the location of the measurement points allows us to study structures and phenomena at a scale rarely investigated. The novel results produced by this work demonstrate the value of such an approach to the study of the hydrothermal activity of an active volcano.

Intense and shallow hydrothermal activity in the Pizzo–Fossa area is clearly shown by the presence of large positive SP, temperature and CO_2 anomalies. These anomalies are focused on crater faults that thus appear to constitute the most permeable medium of the zone. The analysis of the distribution of these linear anomalies, coupled with the examination of the geologic, photographic and topographic data, has led us to propose a new structural interpretation of the summit of Stromboli. This newly defined structural framework comprises the following:

1. A large Pizzo circular crater, about 350 m in diameter.
2. A complex of now concealed nested craters within the Pizzo crater (the Large and the Small Fossa craters) that are thought to have formed during the eruption of the Pizzo pyroclastites unit. The Small Fossa crater is filled with impermeable material that totally impedes the upward flow of hydrothermal fluids.
3. The complex of presently active craters.

On the floor of the Fossa, short wavelength SP lows are arranged in drainage-like networks diverging from the main thermal anomalies and converging toward the Small Fossa crater. They are thought to show the subsurface downhill flow of water condensed above thermal anomalies. The water can form a perched reservoir at shallow depth. The inferred presence of a large quantity of water near the active zone constitutes a major hazard because phreatic and phreatomagmatic activity can occur if magma intrudes into this area. It is possible that such a phenomenon occurred during the 1930 phreatic paroxysm.

A striking result of the survey is the high correlation between T and CO_2 anomalies in this context. The two types of anomalies have very similar shapes, but the sensibility of CO_2 measurements seems better because in some areas clear CO_2 anomalies could still be detected when the subsurface temperature measurements did not show significant signals. At T anomalies, a higher amplitude of high frequency SP signal is observed.

Geochemical analyses of the fluids show the similarity of composition between the gases rising through the faults of the Pizzo and Fossa craters. This suggests a common origin for the gases emerging along the different structural paths in the summit of Stromboli. A site has been identified along the Large Fossa crater fault (anomaly F1) where high gas flux and weak air contamination make possible the future monitoring of gases near the active vents using the alkaline bottle sampling technique.

Acknowledgements We are grateful to Franco Barberi for providing us with an Italian Civil Protection helicopter to carry scientific materials and food to the summit of Stromboli during the summer of 1995. We sincerely thank Jean-Marie Barnagaud and Thierry Challan for help during the 1992 and 1994, respectively, summer preliminary campaigns, Yashmin Chébli and Sébastien Durand for their invaluable help during the 1995 summer campaign, and Sandrine Poteaux and Virginie Meister during the 1999 summer campaign. We greatly thank John Murray for his help to improve the English. Reviews by Steve Lane and Giorgio Cassiani have helped to improve the manuscript. A.F. acknowledges Klaus Gwinner from DLR—Institute of Space Sensor Technology and Planetary Exploration, for providing airborne photographs of Stromboli Volcano. A.F. also acknowledges the Société de Secours des Amis des Sciences for a research grant, and particularly thanks Jean Todt (Sports Director of Formula One Scuderia Ferrari), Giancarlo Minardi (Director of the Minardi Formula One team), Flavio Briatore, (Director of the Formula One Benetton team) and Marc Demougeot (Director of Sparco-France) for their help into obtaining Formula One fireproof equipment. Without it, measurements near the active craters could not have been carried out for security reasons.

References

Allard P, Hammouya G, Parello F (1998) Diffuse magmatic soil degassing at Soufrière of Guadeloupe, Antilles. C R Acad Sci Paris 327:315–318

Alparone S, Cocina O, Falsaperla S, Patanè D, Privitera E, Spampinato S (1999) Aeolian Islands, Stromboli : seismicity. Volcanology and chemistry of the Earth's interior. Italian Research Activity (1995–1998) report to IAVCEI. Boll Geofis Appl 40:222–224

Aubert M (1999) Practical evaluation of steady heat discharge from dormant active volcanoes : case study of Vulcarolo fissure (Mount Etna, Italy). J Volcanol Geotherm Res 92:413–429

Aubert M, Atangana Q (1996) Self-potential method in hydrogeological exploration of volcanic areas. Ground Water 34:1010–1016

Aubert M, Baubron JC (1988) Identification of a hidden thermal fissure in a volcanic terrain using a combination of hydrothermal convection indicators and soil-atmosphere analysis. J Volcanol Geotherm Res 35:217–225

Aubert M, Dana I (1994) Interprétation des profils radiaux de polarisation spontanée (PS) en volcanologie. Possibilités d'ap-

plication de la méthode PS à la surveillance des volcans actifs. Bull Soc Géol France 165:113–122
Aubert M, Auby R, Bourley F, Bourley Y (1984) Contribution à la surveillance de l'activité de l'Etna à partir de l'étude des zones fumeroliennes. Bull Volcanol 47:1039–1050
Aubert A, Dana I, Livet M (1990) Identification of the boundaries between two watersheds in a volcanic area by self-potential method. C R Acad Sci Paris 311:990–1004
Aubert M, Dana I, Dupuy JC (1991) Application of the self-potential method to the detection of underground water courses in a volcanic area. C R Acad Sci Paris 312:325–330
Aubert M, Antraygues P, Soler E (1993) Interpretation of the self-potential measurements in hydrogeological exploration of a volcanic massif. On the existence of groundwater flow paths on the south flank of the Piton de la Fournaise (Réunion Island). Bull Soc Géol France 164:17–25
Azzaro R, Branca S, Giammanco S, Gurrieri S, Rasà R, Valenza M (1998) New evidence for the form and extent of the Pernicana Fault System (Mt Etna) from structural and soil-gas surveying. J Volcanol Geotherm Res 84:143–152
Ballestracci R (1982a) Self-potential survey near the craters of Stromboli volcano (Italy). Inference for internal structure and eruption mechanism. Bull Volcanol 45:349–365
Ballestracci R (1982b) Audiomagnetotelluric profiling on the volcano Stromboli, internal structure and mechanism of the strombolian activity. J Volcanol Geotherm Res 12:317–337
Barberi F, Rosi M, Sodi A (1993) Volcanic hazard assessment at Stromboli based on review of historical data. Acta Vulcanol 3:173–187
Barberi F, Carapezza ML (1994) Helium and CO_2 soil gas emission from Santorini (Greece). Bull Volcanol 56:335–342
Bertagnini A, Coltelli M, Landi P, Pompilio M, Rosi M (1999) Violent explosions yield new insights into dynamics of Stromboli volcano. EOS Trans Am Geophys Union 80:633–636
Bonaccorso A, Gambino S, Puglisi G, Mattia M, Velardita R, Villari L (1999) Aeolian Islands, Stromboli: ground deformation. Volcanology and chemistry of the Earth's interior. Italian Research Activity (1995–1998) report to IAVCEI. Boll Geofis Appl 40:224–226
Bullard FM (1954) Activity of Stromboli in June and December 1952. Bull Volcanol 15:91–98
Braun T, Neuberg J, Ripepe M (1996) On the origin of the long-period tremor recorded at Stromboli Volcano (Italy). Ann Geof 39:311–326
Carapezza ML, Federico C (2000) The contribution of fluid geochemistry to the volcano monitoring of Stromboli. J Volcanol Geotherm Res 95:227–245
Chébli Y (1997) Tomographie thermique et géoélectrique du cratère du Vulcano. Mémoire de DEA Processus Magmatiques et Métamorphiques—Volcanologie, Université Blaise Pascal, Clermont-Ferrand II
Coltelli M, Pompilio M, Del Carlo P (1999) Aeolian Islands, Stromboli : volcanic activity. Volcanology and chemistry of the Earth's interior. Italian Research activity (1995–1998) report to IAVCEI. Italian research activity (1995–1998) report to IAVCEI. Boll Geof Appl 40:217–222
Corwin RF, Hoover DB (1979) The self-potential method in geothermal exploration. Geophysics 44:226–245
D'Alessandro W, De Domenico R, Parello F, Valenza M (1992) Soil degassing in tectonically active areas of Mt Etna. Acta Vulcanol 2:175–183
Di Maio R, Patella D (1994) Self-potential anomaly generation in volcanic areas. The Mt Etna case-history. Acta Vulcanol 4:119–124
Ernstson K, Scherer H (1986) Self-potential variations with time and their relation to hydrogeologic and meteorological parameters. Geophysics 51:1967–1977
Etiope G, Beneduce P, Calcara M, Favali P, Frugoni F, Schiattarella M, Smriglio G (1999) Structural pattern and CO_2–CH_4 degassing of Ustica Island, Southern Tyrrhenian basin. J Volcanol Geotherm Res 88:291–304
Finizola A (1996) Etude d'une fissure thermique au Stromboli; interprétation volcanologique et structurale. Mémoire de DEA Processus Magmatiques et Métamorphiques—Volcanologie, Université Blaise Pascal, Clermont-Ferrand II
Finizola A, Ramos D, Macedo O (1998) Self-potential studies of hydrothermal systems and structure on Misti and Ubinas volcanoes, South Peru. In: Geophysicae A (ed) 23rd EGS Meeting. Solid Earth Geophysics and Geodesy, Nice
Finizola A, Sortino F, Lénat JF, Valenza M (2002) Fluid circulation at Stromboli volcano (Aeolian Island, Italy), from self-potential and CO_2 surveys. J Volcanol Geotherm Res 116(1–2):1–18
Francalanci L (1987) Evoluzione vulcanologica e magmatologica dell'isola di Stromboli (Isole Eolie): Relazioni tra magmatismo calc-alcalino e shoshonitico, Tesi di dottorato, Università di Firenze, Firenze
Gabbianelli G, Romagnoli C, Rossi PL, Calanchi N (1993) Marine geology of the Panarea—Stromboli area (Aeolian Archipelago, Southeastern Tyrrhenian sea). Acta Vulcanol 3:11–20
Giammanco S, Gurrieri S, Valenza M (1997) Soil CO_2 degassing along tectonic structures of Mount Etna (Sicily): the Pernicana fault. Appl Geochem 12:429–436
Giammanco S, Gurrieri S, Valenza M (1998) Anomalous soil CO_2 degassing in relation to faults and eruptive fissures on Mount Etna (Sicily, Italy). Bull Volcanol 60:252–259
Giggenbach WF (1975) A simple method for the collection and analysis of volcanic gas samples. Bull Volcanol 39:15–27
Gillot PY (1984) Datation par la méthode potassium argon des roches volcaniques récentes (pléistocènes et holocènes). Contribution à l'étude chronostratigraphique et magmatique des provinces volcaniques de Campanie, des Iles Eoliennes, de Pantelleria (Italie du Sud) et de la Réunion (Océan Indien). PhD Thesis, Paris XI-Orsay
Gillot PY, Keller J (1993) Radiochronological dating of Stromboli. Acta Vulcanol 3:69–77
Gwinner K, Hauber E, Jaumann R, Neukum G (2000) High-resolution, digital photogrammetric mapping : a tool for earth science. EOS Trans Am Geophys Union 81:515–520
Hornig-Kjarsgaard I, Keller J, Koberski U, Stadlbauer E, Francalanci L, Lenhart R (1993) Geology, stratigraphy and volcanological evolution of the island of Stromboli, Aeolian Arc, Italy. Acta Vulcanol 3:21–68
Jackson DB, Kauahikaua J (1987) Regional self-potential anomalies at Kilauea volcano. Volcanism in Hawaii, ch 40. US Geol Survey Prof Pap 1350:947–959
Keller J, Hornig-Kjarsgaard I, Koberski U, Stadlbauer E, Lenhart R (1993) Geological map of the island of Stromboli. Acta Vulcanol 3
Lénat JF, Robineau B, Durand S, Bachélery P (1998) Etude de la zone sommitale du volcan Karthala (Grande Comore) par polarisation spontanée. C R Acad Sci 327:781–788
Malengreau B, Lénat JF, Bonneville A (1994) Cartographie et surveillance temporelle des anomalies de Polarisation Spontanée (PS) sur le Piton de la Fournaise. Bull Soc Géol Fr 165:221–232
Martini M (1991) Stromboli, report activity. Bull Global Volcanism Network 16:20–21
Matsushima N, Michiwaki M, Okazaki N, Ichikawa N, Takagi A, Nishida Y, Mori HY (1990) Self-potential study in volcanic areas—Usu, Hokkaido Komaga-take and Me-akan. J Fac Sci Hokkaido Univ Ser VII (Geophysics) 8:465–477
Nishida Y, Tomiya H (1987) Self-potential studies in volcanic areas—Usu volcano. J Fac Sci Hakkaiodo Univ Ser VII (Geophysics) 8:173–190
Papale P (1999) Modeling of the solubility of a two-component $H_2O + CO_2$ fluid in silicate liquids. Am Mineral 84:477–492
Pasquarè G, Francalanci L, Garduno VH, Tibaldi A (1993) Structure and geologic evolution of the Stromboli volcano, Aeolian Islands, Italy. Acta Vulcanol 3:79–89
Patella D (1997) Self-potential global tomography including topographic effects. Geophys Prospect 45:843–863

Ripepe M (1996) Evidence of gas influence on volcanic seismic signals recorded at Stromboli. J Volcanol Geotherm Res 70:221–233

Ripepe M, Gordeev E (1999) Gas bubble dynamics model for shallow volcanic tremor at Stromboli. J Geophys Res B Solid Earth Planet 104:10639–10654

Ripepe M, Rossi M, Saccorotti G (1993) Image processing of explosive activity at Stromboli. J Volcanol Geotherm Res 54:335–351

Ripepe M, Poggi P, Braun T, Gordeev E (1996) Infrasonic waves and volcanic tremor at Stromboli. Geophys Res Lett 23:181–184

Ripepe M, Ciliberto S, Schiava MD (2001) Time constraints for modeling source dynamics of volcanic explosions at Stromboli. J Geophys Res B Solid Earth Planet 106:8713–8727

Rittmann A (1931) Der Ausbruch des Stromboli am 11 september 1930. Zeits Vulkanol 14:47–77

Rosi M (1980) The island of Stromboli. Rend Soc It Mineral Petrol 36:345–368

Sano Y, Tominaga T, Nakamura Y, Wakita H (1982) $^{3}He/^{4}He$ ratios of methane-rich natural gases in Japan. Geochem J 16:237–245

Schiavone D, Quarto R (1984) Self-potential prospecting in the study of water movements. Geoexploration 22:47–58

Sill WR (1983) Self-potential modeling from primary flows. Geophysics 48:76–86

Tibaldi A (2001) Multiple sector collapse at Stromboli volcano, Italy: how they work. Bull Volcanol 63:112–125

Zablocki CJ (1976) Mapping thermal anomalies on an active volcano by the self-potential method, Kilauea, Hawaii. Proceedings, 2nd UN Symposium of the development and use of geothermal resources, San Francisco, May 1975, pp 1299–1309

Zablocki CJ (1978) Streaming potentials resulting from the descent of meteoric water. A possible source mechanism for Kilauean self-potential anomalies. Geotherm Resour Council Trans 2:747–748

Zanchi A, Francalanci L (1989) Analisi geologico-strutturale dell'isola di Stromboli: alcune considerazioni preliminari. Boll GNV 5:1027–1044

Zlotnicki J, Michel S, Annen C (1994) Anomalies de polarisation spontanée et systèmes convectifs sur le volcan du Piton de la Fournaise (Ile de la Réunion, France). C R Acad Sci Paris 318:1325–1331